Japanese Journal of Applied Physics **58**, SC1004 (2019)

REGULAR PAPER

https://doi.org/**10.7567/1347-4065/ab07a4**

Indium incorporation in quaternary $In_xAl_yGa_{1-x-y}N$ for UVB-LEDs

Johannes Enslin[1*], Tim Wernicke[1], Anna Lobanova[2], Gunnar Kusch[3], Lucia Spasevski[3], Tolga Teke[1], Bettina Belde[1], Robert W. Martin[3], Roman Talalaev[2], and Michael Kneissl[1]

[1]*Technische Universität Berlin, Institute of Solid State Physics, 10623 Berlin, Germany*
[2]*STR Group Inc., 194044 St. Petersburg, Russia*
[3]*Department of Physics, SUPA, University of Strathclyde, Glasgow G4 0NG, United Kingdom*

[*]E-mail: johannes.enslin@physik.tu-berlin.de

Received December 14, 2018; revised January 14, 2019; accepted January 22, 2019; published online April 16, 2019

Consistent studies of the quaternary composition are rare as it is impossible to fully determine the quaternary composition by X-ray diffraction or deduce it from that of ternary alloys. In this paper we determined the quaternary composition by wavelength dispersive X-ray spectroscopy of $In_xAl_yGa_{1-x-y}N$ layers grown by metal organic vapor phase epitaxy. Further insights explaining the peculiarities of $In_xAl_yGa_{1-x-y}N$ growth in a showerhead reactor were gained by simulations of the precursor decomposition, gas phase adduct formation and indium incorporation including desorption. The measurements and simulations agree very well showing that the indium incorporation in a range from 0% to 2% is limited by desorption which is enhanced by the compressive strain to the relaxed $Al_{0.5}Ga_{0.5}N$ buffer layer as well as indium incorporation into AlN particles forming in the gas phase. Utilizing $In_xAl_yGa_{1-x-y}N$ layers containing 2% of indium for multiple quantum wells (MQWs), it was possible to show an almost five times higher photoluminescence intensity of InAlGaN MQWs in comparison to AlGaN MQWs.

1. Introduction

Ultraviolet light in the range between 280 and 320 nm (UVB) is needed for a number of applications, such as plant growth lighting,[1)] and phototherapy for the treatment of psoriasis and vitiligo.[2)] Light emitting diodes (LEDs) emitting in this spectral region are superior to conventional light sources like Hg-lamps due to high spatial purity, freely selectable wavelength, long lifetime, small size, and environmental friendliness. Nevertheless, these devices still suffer from relatively low external quantum efficiencies.[3)]

Quaternary $In_xAl_yGa_{1-x-y}N$ alloys are of great interest for high efficiency III-nitride based devices adding a new degree of freedom for the engineering of bandgap and band offsets, strain, polarization fields, carrier localization, and crystal field, e.g. for the quantum well design of UVB-LEDs. Hirayama et al. showed that the photoluminescence (PL) intensity of UVB emitting multiple quantum wells (MQWs) could be increased by using $In_xAl_yGa_{1-x-y}N$ MQWs instead of $Al_yGa_{1-y}N$ MQWs[4)]. However, consistent studies of the quaternary composition are rare as it is impossible to fully determine the quaternary composition by X-ray diffraction or deducing it from the ternary alloys. However, one of the challenges is growing InAlGaN layers at the appropriate growth temperature. On the one hand AlGaN layers are generally grown at temperatures above 1000 °C[5,6)] due to low diffusion length on the surface which can be increased by elevated temperatures.[7)] On the other hand InGaN[8,9)] and InAlN[10,11)] layers are typically grown below 880 °C in order to limit the desorption of In atoms from the surface.[12)]

In this paper we study the composition of $(In_x)Al_yGa_{1-x-y}N$ layers grown by metal organic vapor phase epitaxy at different growth temperatures, by wavelength dispersive X-ray spectroscopy (WDX) as well as high resolution X-ray diffraction (HRXRD) reciprocal space maps (RSM). Further insights explaining the peculiarities of $In_xAl_yGa_{1-x-y}N$ growth were gained by simulations of the precursor decomposition, gas phase adduct formation and indium incorporation including (strain induced) desorption.

2. Experimental

The investigated $(In_x)Al_yGa_{1-x-y}N$ layers were grown by metalorganic vapor phase epitaxy in a close coupled showerhead reactor. AlN/sapphire templates[13)] are used as substrates with a subsequently grown AlN/AlGaN-superlattice (SL) for strain management and a relaxed $Al_{0.5}Ga_{0.5}N$ buffer layer acting as a quasi-substrate[14,15)] for further growth with a threading dislocation density of about $2 \times 10^9 cm^{-2}$. The $(In_x)Al_yGa_{1-x-y}N$ layers were grown with N_2 as carrier gas under a pressure of 400 mbar. As precursors Trimethylindium (TMIn) with a flux of 17.3 μmol min^{-1}, Trimethylaluminum (TMAl) with a flux of 26.5 μmol min^{-1}, Trimethylgallium (TMGa) with a flux of 8.9 μmol min^{-1} and ammonia (NH_3) with a flux of 89.3 mmol min^{-1} were used, resulting in a V/III-ratio of 1700. To contain the interaction volume within the InAlGaN layer, for the WDX measurements, the thickness of the $(In_x)Al_yGa_{1-x-y}N$ layers was chosen to be 150 nm. The growth temperature was varied between 790 °C and 930 °C. For a better comparison $Al_yGa_{1-y}N$ layers were grown under identical conditions at temperatures between 820 °C and 900 °C without supplying TMIn during growth. The growth rate of all layers was monitored by an in situ reflectance setup. After growth, the strain state of the samples was analyzed using HRXRD RSMs of the asymmetric (10.5) reflection. For AlGaN the composition was analyzed by the same method.

WDX measurements were carried out in a JEOL JXA–8530F electron probe microanalyser to determine the composition of all samples, using AlN, GaN and InP as standards. The measurements were performed with a beam current of 40 nA, 5 kV acceleration voltage and a beam defocused to a spot size of 10 μm. Carbon coating of the samples was necessary as charging effects were observed during initial measurements; samples were coated with carbon of similar thickness as the standards. According to Monte Carlo simulations using CASINO software,[16)] approximately 90% of the beam energy is deposited in the first 80 nm of an $Al_{0.35}Ga_{0.75}N$ layer at the chosen acceleration voltage. The

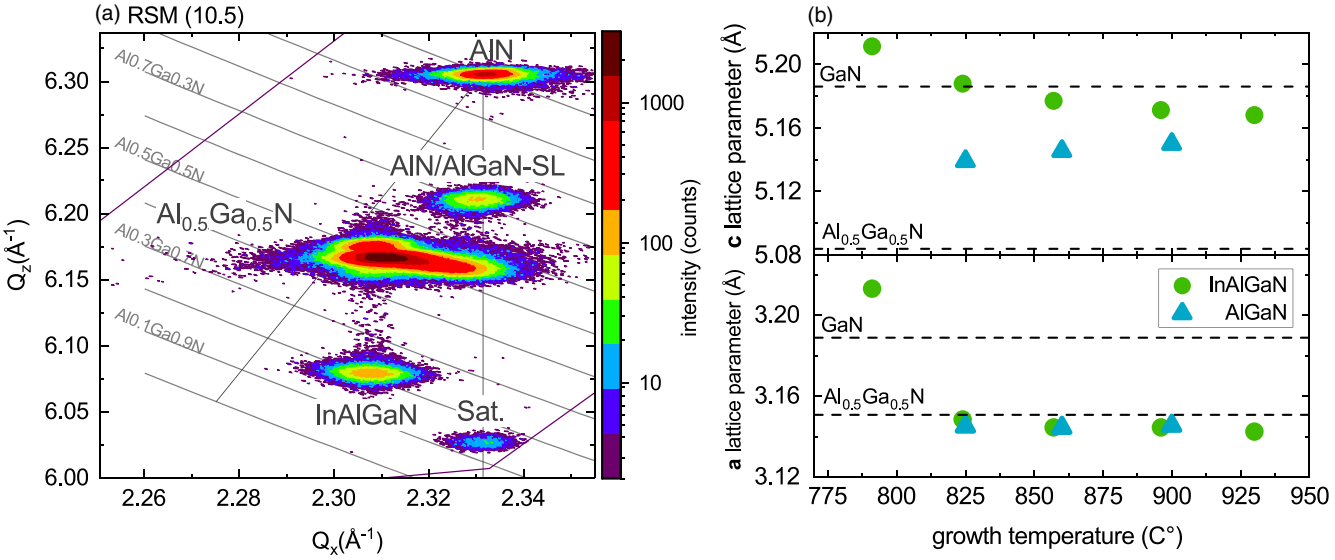

Fig. 1. (Color online) HRXRD RSM near the (10.5) reflection of AlN (a). Showing the $Al_{0.5}Ga_{0.5}N$-template structure with the subsequently grown $In_xAl_yGa_{1-x-y}N$ layer at a growth temperatures of 930 °C. Calculated a and c lattice parameters (b) of $(In_x)Al_yGa_{1-x-y}N$ layers obtained from RSMs with reference values for unstrained GaN and $Al_{0.5}Ga_{0.5}N$.

beam energy is well above the minimum energy needed to excite the selected X-ray lines while containing the interaction volume within the desired layer, as for lower AlN% (higher InN%) the penetration depth of the electron beam will be smaller due to the higher material density.

Growth rate and composition were simulated by the STR group by modeling the gas and surface chemistry taking gasflow, temperature and strain of the layer into account.[17–19] In an additional experiment, MQWs containing InAlGaN quantum wells and AlGaN barriers in between were compared to pure AlGaN MQWs. First a 40 nm thick first barrier was grown at 900 °C, followed by a threefold MQW with QW widths of 2 nm grown at 825 °C and capped by a 15 nm last barrier (grown at 900 °C). The energetic offset between QW and barrier was kept constant at 230 meV. The estimated composition of the InAlGaN quantum well is $In_{0.02}Al_{0.30}Ga_{0.68}N$ and the AlGaN quantum well consists of an $Al_{0.25}Ga_{0.75}N$ layer. The grown structures were investigated by PL using an argon fluoride excimer laser with a wavelength of 193 nm and an excitation power density of 90 kW cm^{-2}.

3. Results and discussion

3.1. Strain and composition of $In_xAl_yGa_{1-x-y}N$

Figure 1(a) shows the HRXRD RSM of the (10.5) reflections of an $In_xAl_yGa_{1-x-y}N$ layer grown at a temperature of 930 °C on top of an $Al_{0.5}Ga_{0.5}N$ pseudo substrate which causes most of the peaks in the RSM. The AlN/AlGaN-SL is grown pseudomorphically on top of a AlN/sapphire substrate indicated by a reflection at the same Q_x-value as AlN. The $Al_{0.5}Ga_{0.5}N$ layer shows a broad peak indicating relaxation within the layer. RSMs were conducted for all grown InAlGaN and AlGaN samples. By determining the position of each layer within reciprocal space the a and c lattice parameters are extracted. Figure 1(b) shows the dependence of these lattice parameters on the growth temperature alongside those for unstrained GaN and $Al_{0.5}Ga_{0.5}N$. For InAlGaN layers grown at temperatures between 930 °C and 820 °C as well as AlGaN layers grown at temperatures between 900 °C and 820 °C the determined a lattice constants are similar to those of the underlying $Al_{0.5}Ga_{0.5}N$. Furthermore, a trend of increasing c lattice parameters with decreasing growth temperature is observed for InAlGaN layers and indicates an increased incorporation of Ga and/or In into the layer. Contrary to that, the AlGaN layers [triangles in Fig. 1(b)] show a decrease of the c lattice parameter with decreasing growth temperature, indicating a decreasing Al-content. The InAlGaN layer grown at 790 °C behaves very differently to the other samples, with a and c lattice parameters larger than those of GaN and large broadening in the Q_x-direction (not shown here). As the relaxation ($a = 3.213\,3$ Å) affects the In-incorporation, this layer will be excluded from the analysis below and will be discussed in more detail in Sect. 4.

Since determining the composition of InAlGaN by HRXRD is not possible, WDX measurements were performed.[20] Figure 2 shows the In-, Al-, and Ga-content of the grown $In_xAl_yGa_{1-x-y}N$ layers (green circles) and $Al_yGa_{1-y}N$ layers (blue triangles) at different growth conditions as determined by WDX. Furthermore, results for the composition of $In_xAl_yGa_{1-x-y}N$ by simulation of the gas and surface chemistry are shown. The simulation that takes account of prereactions, including the formation of particles, fits very well to the experimentally obtained data in contrast to the simulation which does not consider the foramtion of particles, see Fig. 2(a). These findings will be discussed in more detail in the next section. Figures 2(b) and 2(c) show the results for WDX measurements of AlGaN layers. The composition of the grown AlGaN layers increases with decreasing growth temperature from 29% at 900 °C to 34% at 825 °C. HRXRD investigations show a similar result (not shown here) showing the good agreement between WDX and HRXRD which was already shown by Kusch et al.[21] Interestingly, the Al-content of InAlGaN layers grown under the same conditions and at the same temperatures is drastically decreased down to 18% to 22% compared to AlGaN layers. This result clearly shows that it is not possible to deduce the quaternary composition from the ternary one. Figure 2(a) shows an increasing In-content with decreasing

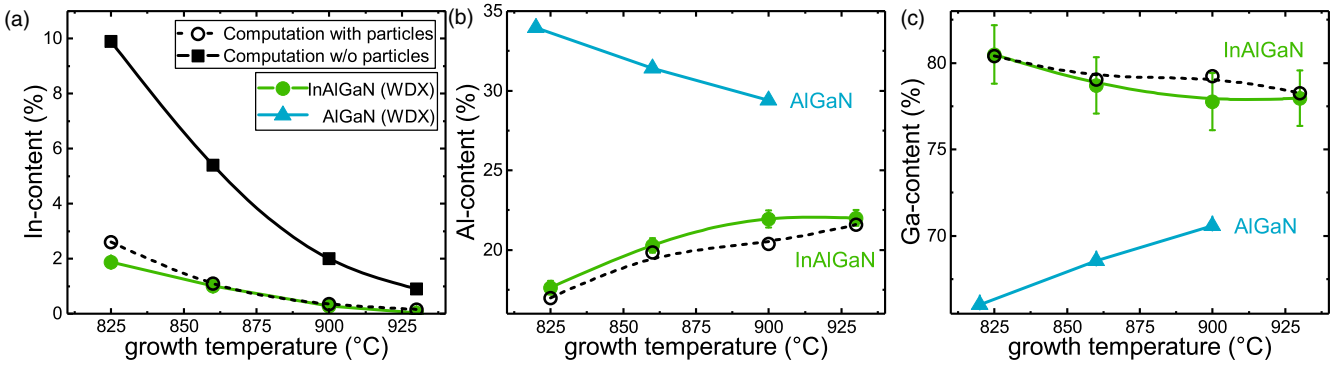

Fig. 2. (Color online) In-, Al-, Ga-content versus the growth temperature of $(In_x)Al_yGa_{1-x-y}N$ layers determined by WDX and simulation of the gas and surface chemistry.

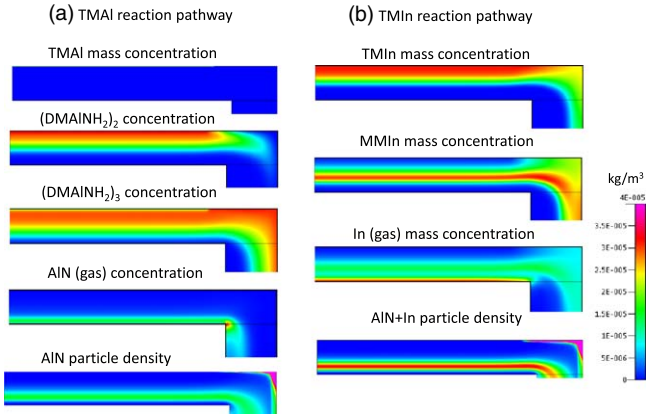

Fig. 3. (Color online) Simulation of the TMAl (a) and TMIn (b) decomposition pathways in a close coupled showerhead reactor.

growth temperature from 0.03% at 930 °C to 1.9% at 825 °C. Accordingly, the Ga-content of InAlGaN layers increases with decreasing growth temperature.

Although, InAlGaN and AlGaN layers show similar growth rates for higher temperatures (860 °C and 900 °C) between 0.080 μm h^{-1} and 0.103 μm h^{-1} the growth rate is increased by 40% for InAlGaN grown at 825 °C. These findings can be explained by an additional Ga supply to the substrate. A similar behavior was already observed for the unitentional incorporation of Ga in InAlN layers.[22–24] This supply is formed by the decomposition of parasitic Ga-containing residues on the showerhead via In-radicals.

3.2. Indium incorporation mechanisms in $In_xAl_yGa_{1-x-y}N$

In order to reach a deeper understanding of the In-incorporation mechanisms, simulations of gas and surface kinetics were performed. Using the reactor conditions stated earlier as input parameters, temperatures, gasflow, gasphase reactions and surface reactions are calculated enabling estimation of the growth rate and composition of InAlGaN. The results of this simulation are shown in Fig. 2. The computation considering prereactions including the formation of particles resembles very well the experimentally found values for the In-, Al- and Ga-content. As shown in Fig. 2(a) the computation not considering particles shows a much higher In-incorporation and does not fit to the experimentally found data. The same behavior is true for the Al and Ga, therefore these computations are not shown in Figs. 2(b) and 2(c). A further insight into the reaction pathways of the mainly occurring species is gained by 2D-simulations of the reactor cross section. The reaction pathway of TMAl is shown in Fig. 3(a). The TMAl decomposes rapidly and reacts with NH_3 to the oligomers $(DMAlNH_2)_2$ and $(DMAlNH_2)_3$. These products decompose to gaseous AlN which shows the highest concentration close to the susceptor, but a notable concentration minimum directly at the substrate surface. This observation indicates efficient incorporation of Al into the semiconductor. Figure 3(b) shows the raction pathway of TMIn, which decomposes to MMIn with the highest concentration in the center of the gap between showerhead and susceptor. Further decomposition leads to In, with a highest concentration directly above the wafer showing strong desorption at elevated temperatures. Due to the relatively high pressure of 400 mbar and high V/III-ratio, AlN particles[25–27] are formed at a similar position in the reactor as gaseous AlN. It is assumed that Al- and In-containing species (MMIn and In) stick to initially nucleated AlN particles. A notable minimum of indium occurs at the position of the highest AlN particle concentration. AlN particles incorporate In from the gasphase leading to In-containing particles with a density exceeding the density of pure AlN particles [Figs. 3(a) and 3(b)]. This consumption of In by the particles reduces the available In atoms in the gas-phase. The simulations show that the In incorporation could be increased by a factor of five by suppressing these prereactions. Furthermore, Al is also consumed by In-containing AlN particles and therefore the Al composition of InAlGaN is further reduced in comparison to AlGaN layers [shown in Fig. 2(b)].

The strain state plays an important role in the incorporation of In, which is illustrated in Fig. 4. The simulated In-content of $In_xAl_yGa_{1-x-y}N$ layers is plotted against the lateral lattice constant for temperatures of 790 °C and 825 °C. Both curves show an increasing In incorporation with increased lateral lattice constant. The experimentally determined In content [see Fig. 2(a)] of the InAlGaN layer grown at 825 °C and the a lattice constant (see Fig. 1) show a very good agreement with the simulated In incorporation. Furthermore, the InAlGaN layer grown at 790 °C, which was excluded from the analysis so far, was analyzed for this evaluation. WDX measurements of this layer show an In-content of 14.6%, Al-content of 24.8% and a Ga-content of 60.6%. Figure 1 already showed a strong relaxation of this layer to the underlying AlGaN-template, resulting in a large a lattice parameter of 3.21 Å. Again, the experimental data point fits very well to the simulated In incorporation at 790 °C. It is

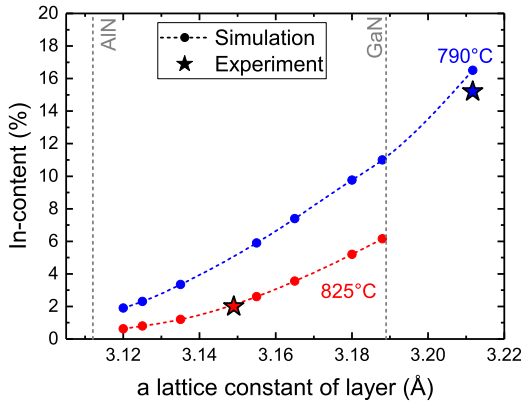

Fig. 4. (Color online) Simulation of the In-incorporation of $In_xAl_yGa_{1-x-y}N$ layers in dependence of the lateral lattice constant for a growth temperature of 790 °C and 825 °C illustrating the strain dependence of the In-incorporation.

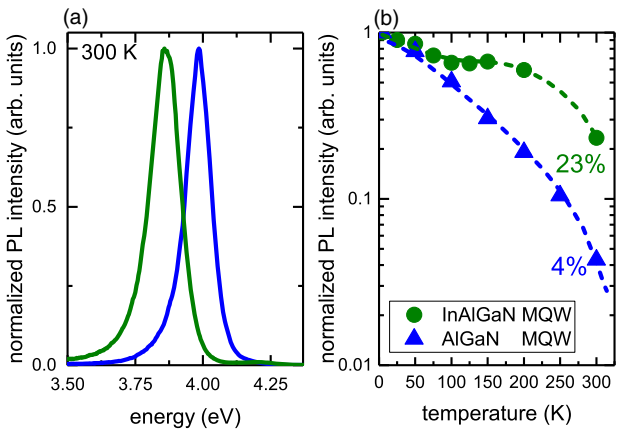

Fig. 5. (Color online) (a) Normalized PL spectra at room temperature and (b) temperature dependent intensity of InAlGaN and AlGaN MQWs normalized to the value at 5 K.

shown that not only the temperature influences the In incorporation drastically but also the strain state.

The main factor for In incorporation can be summarized as follows: The In incorporation is influenced by the loss of In precursors due to prereactions and the desorption of In from the surface which is further enhanced by compressive strain. As strain is typically defined by the layers underneath the InAlGaN layer, the In incorporation could be enhanced by reducing the growth temperature further and suppressing prereactions by lowering the pressure, decreasing the NH_3 flow, increasing the total flow or reducing the gap between showerhead and susceptor.[28)]

3.3. Optical properties of MQWs

In order to emphasize the relevance of InAlGaN layers we grew InAlGaN and AlGaN MQWs and investigated the temperature dependent PL. Figure 5(a) shows the PL spectra recorded at 300 K. Both structures show single peak PL emission between 3.8 eV and 4.0 eV. Furthermore, the temperature dependent PL intensity is plotted in Fig. 5(b). The MQW consisting of pure AlGaN layers shows the expected behavior of a decreasing normalized PL intensity with increasing temperature resulting in a 300 K emission intensity reduced to 4% of the emission intensity at low temperature. Contrary to that, the InAlGaN containing MQW shows a very different trend. In the low temperature regime between 0 and 50 K the PL intensity decreases as expected, after that, it stays constant for the next 100 K. Subsequently, the PL intensity decreases again with increasing temperature, resulting in a 300 K intensity reduced to 23% of the low temperature value, which is most likely due to compositional fluctuations within the InAlGaN MQWs[29)] which create enhanced carrier localization and increased recombination efficiencies.[30)] This experiment shows an overall smaller decrease of the temperature dependent PL intensity for InAlGaN MQWs in comparison to AlGaN MQWs. Similar results are reported in literature, for example Ref. 31 observed no room temperature PL for pure AlGaN MQWs, but an increased ratio of 10 K PL intensity to room temperature PL intensity with increasing In-content in the active layers.

4. Conclusion

This work provides details of the In-incorporation in InAlGaN layers grown on relaxed $Al_{0.5}Ga_{0.5}N$ pseudo substrates suitable for UVB-LED growth in a close coupled showerhead reactor. By a variation of the growth temperature for InAlGaN and AlGaN layers we could increase the In-content from 0.03% to 1.9%, determined by WDX. Furthermore, we used reactor simulations to confirm these results and get a deeper understanding of the limiting factors for the In-incorporation. We were able to show, that not only desorption due to elevated temperatures, but also gas phase prereactions forming AlN + In particles decrease the In supply to the substrate by a factor of five. Moreover, strain induced desorption limits the In-incorporation again by a factor of five. In addition, it was shown that radicals formed during TMIn decomposition dissolve Ga-deposits on the showerhead surface leading to an additional Ga-supply to the substrate and prevent deduction of the quaternary composition from that of the ternaries. Finally it was demonstrated that the implementation of InAlGaN layers in MQWs can lead to an increased PL intensity in comparison to pure AlGaN MQWs.

Acknowledgments

The authors would like to thank Sylvia Hagedorn (Ferdinand-Braun-Institut, Berlin) for providing AlN/sapphire templates and Praphat Sonka (Technische Universität Berlin) for technical support. This work was partially supported by the German Federal Ministry of Education and Research (BMBF) within the "Advanced UV for Life" project and by the Deutsche Forschungsgemeinschaft (DFG) within the Collaborative Research Center "Semiconductor Nanophotonics" (SFB 787).

1) M. Schreiner, J. Martinez-Abaigar, J. Glaab, and M. Jansen, Optik Photonik **9**, 34 (2014).
2) W. Morison, *Phototherapy and Photochemotherapy of Skin Disease* (Raven Press, New York, 1991) 2nd ed.
3) M. Kneissl and J. Rass, *III-Nitride Ultraviolet Emitters—Technology and Applications* (Spinger, Berlin, 2016) Springer Series in Material Science, Vol. 227.
4) H. Hirayama, J. Appl. Phys. **97**, 091101 (2005).
5) A. V. Lobanova, K. M. Mazaev, R. A. Talalaev, M. Leys, S. Boeykens, K. Cheng, and S. Degroote, J. Cryst. Growth **287**, 601 (2006).
6) N. Okada et al., Jpn. J. Appl. Phys. **45**, 2502 (2006).
7) S. Nitta, Y. Yukawa, Y. Watanabe, S. Kamiyama, H. Amano, and I. Akasaki, Phys. Status Solidi A **194**, 485 (2002).

8) H. P. D. Schenk, P. de Mierry, M. Laügt, F. Omnés, M. Leroux, B. Beaumont, and P. Gibart, Appl. Phys. Lett. **75**, 2587 (1999).
9) M. Bosi and R. Fornari, J. Cryst. Growth **265**, 434 (2004).
10) H. P. D. Schenk, M. Nemoz, M. Korytov, P. Vennegues, A. D. Dräger, and A. Hangleiter, Appl. Phys. Lett. **93**, 081116 (2008).
11) G. Liu, J. Zhang, G. S. Huang, T. Paskova, K. R. Evans, H. Zhao, and N. Tansu, J. Cryst. Growth **340**, 66 (2012).
12) K. Zhou et al., J. Cryst. Growth **409**, 51 (2015).
13) O. Reentilä, F. Brunner, A. Knauer, A. Mogilatenko, W. Neumann, H. Protzmann, M. Heuken, M. Kneissl, M. Weyers, and G. Tränkle, J. Cryst. Growth **310**, 4932 (2008).
14) J. Enslin et al., J. Cryst. Growth **464**, 185 (2017).
15) A. Mogilatenko, J. Enslin, A. Knauer, F. Mehnke, K. Bellmann, T. Wernicke, M. Weyers, and M. Kneissl, Semicond. Sci. Technol. **30**, 114010 (2015).
16) D. Drouin, A. R. Couture, D. Jolly, X. Tastet, V. Aimez, and R. Gauvin, Scanning **29**, 92 (2007).
17) A. V. Lobanova, A. S. Segal, E. V. Yakovlev, and R. A. Talalaev, J. Cryst. Growth **352**, 199 (2012).
18) Z. Liu et al., J. Cryst. Growth **509**, 50 (2019).
19) M. E. Rudinsky, A. V. Lobanova, S. Yu. Karpov, and R. A. Talalaev, to be published in Jpn. J. Appl. Phys. (2019).
20) K. Bejtka, P. R. Edwards, R. W. Martin, S. Fernández-Garrido, and E. Calleja, J. Appl. Phys. **104**, 073537 (2008).
21) G. Kusch, F. Mehnke, J. Enslin, P. R. Edwards, T. Wernicke, M. Kneissl, and R. W. Martin, Semicond. Sci. Technol. **32**, 035020 (2017).
22) J. Kim et al., J. Cryst. Growth **388**, 143 (2014).
23) M. D. Smith et al., J. Mater. Chem. C **2**, 5787 (2014).
24) M. Hiroki, Y. Oda, N. Watanabe, N. Maeda, H. Yokoyama, K. Kumakura, and H. Yamamoto, J. Cryst. Growth **382**, 36 (2013).
25) J. R. Creighton, W. G. Breiland, M. E. Coltrin, and R. P. Pawlowski, Appl. Phys. Lett. **81**, 2626 (2002).
26) J. R. Creighton, M. E. Coltrin, and J. J. Figiel, Appl. Phys. Lett. **93**, 171906 (2008).
27) J. R. Creighton, G. T. Wang, and M. E. Coltrin, J. Cryst. Growth **298**, 2 (2006).
28) S. Keller, G. Parish, P. T. Fini, S. Heikman, C.-H. Chen, N. Zhang, S. P. DenBaars, U. K. Mishra, and Y.-F. Wu, J. Appl. Phys. **86**, 5850 (1999).
29) H. Hirayama, A. Kinoshita, T. Yamabi, Y. Enomoto, A. Hirata, T. Araki, Y. Nanishi, and Y. Aoyagi, Appl. Phys. Lett. **80**, 207 (2002).
30) M. Jetter, C. Wächter, A. Meyer, M. Feneberg, K. Thonke, and P. Michler, J. Cryst. Growth **315**, 254 (2011).
31) M. Miyoshi, M. Kato, and T. Egawa, Semicond. Sci. Technol. **29**, 075024 (2014).